

# A systematical study of the chiral magnetic effects at the RHIC and LHC energies\*

Bang-Xiang Chen(陈帮祥)<sup>1</sup> Sheng-Qin Feng(冯笙琴)<sup>1,2,1)</sup>

<sup>1</sup>College of Science, China Three Gorges University, Yichang 443002, China

<sup>2</sup>Key Laboratory of Quark and Lepton Physics (MOE) and Institute of Particle Physics, Central China Normal University, Wuhan 430079, China

**Abstract:** Considering the magnetic field response of the QGP medium, we perform a systematical study of the chiral magnetic effect (CME), and make a comparison with the experimental results for the background-subtracted correlator  $H$  at the energies of the RHIC Beam Energy Scan (BES) and the LHC energy. The CME signals from our computations show a centrality trend and beam energy dependence that are qualitatively consistent with the experimental measurements of the charge dependent correlations. The time evolution of the chiral electromagnetic current at the RHIC and LHC energies is systematically studied. The dependence of the time-integrated current signal on the beam energy  $\sqrt{s}$  with different centralities is investigated. Our phenomenological analysis shows that the time-integrated electromagnetic current is maximal near the collision energy  $\sqrt{s} \approx 39$  GeV. The qualitative trend of the induced electromagnetic current is in agreement with the CME experimental results at the RHIC and LHC energies.

**Keywords:** chiral magnetic effect, chiral electromagnetic current, charge separations

**DOI:** 10.1088/1674-1137/44/2/024104

## 1 Introduction

When two heavy ions collide with a non-zero impact parameter, a strong magnetic field with a magnitude of the order of  $eB \sim m_\pi^2$  [1–8] ( $m_\pi$  is the pion mass), is generated in the direction of the angular momentum of the collision. The chirality imbalance should have experimental consequences in such a strong magnetic field. If the chirality is non-zero, the quark spins are locked either parallel or anti-parallel to the magnetic field direction, depending on the quark charge. This would lead to a charge separation in the final state and to an electromagnetic current along the direction of the magnetic field [9–12]. Such charge separation and electromagnetic current phenomena are called the chiral magnetic effect (CME) [13–18].

It has been argued that positive charges separate from negative charges along the direction of the angular momentum of the collision if the P and CP-violating processes occur in QGP generated in relativistic heavy-ion collisions [19, 20]. The directional movement of positive

and negative charges in a strong magnetic field should produce an electromagnetic current, which is an intriguing phenomenon that originates in the interplay of a quantum anomaly with the magnetic field. The electromagnetic current  $\vec{J} = \sigma \vec{B}$  would be induced by the chirality imbalance in an external magnetic field  $\vec{B}$ , where  $\sigma = e^2 \mu_5 / (2\pi^2)$  is the chiral magnetic conductivity and  $\mu_5$  is the chiral chemical potential.

Although there exists an obvious background contamination, it was suggested that signals of charge separation are seen in the relativistic heavy-ion collision data of the STAR [21–23] and PHENIX [24] experimental groups at RHIC, and the ALICE [25] collaboration at the LHC. With a new background subtraction method, the data obtained in the RHIC Beam Energy Scan (BES) [26] by the STAR experimental group further demonstrated the possible existence of the CME signal. It seems that the CME signal in the energy range from 19.6 to 62.4 GeV [26] is more clearer. A new phase of the RHIC energy scan will be performed during 2020, which will allow a more accurate study of CME.

Received 26 September 2019, Published online 23 December 2019

\* Supported by National Natural Science Foundation of China (11875178, 11475068, 11747115), the CCNU-QLPL Innovation Fund (QLPL2016P01) and the Excellent Youth Foundation of Hubei Scientific Committee (2006ABB036)

1) E-mail: fengsq@ctgu.edu.cn



Content from this work may be used under the terms of the Creative Commons Attribution 3.0 licence. Any further distribution of this work must maintain attribution to the author(s) and the title of the work, journal citation and DOI. Article funded by SCOAP<sup>3</sup> and published under licence by Chinese Physical Society and the Institute of High Energy Physics of the Chinese Academy of Sciences and the Institute of Modern Physics of the Chinese Academy of Sciences and IOP Publishing Ltd

In this paper, we consider three important issues: 1) the magnetic field response of the quark gluon plasma (QGP) to the time evolution of the strong magnetic field; 2) the interplay of charge separation with the magnetic field; and 3) the dynamical processes in the chiral magnetic current in response to the time-dependent magnetic field. We choose the simplified KMW model to discuss the charge separation and to compare it with the experimental results at the RHIC and LHC energies. For the study of the electromagnetic current, we take into account the finite frequency response of CME to a time-varying magnetic field, find a significant impact of the QGP medium feedback, and study the generated electromagnetic current as a function of beam energy at RHIC and LHC.

The paper is organized as follows: the magnetic field response of the QGP medium in relativistic heavy-ion collisions is given in Sec. 2. The charge separation at the RHIC and LHC energies is discussed in Sec. 3. In Sec. 4, we use the Kubo formula to compute the electromagnetic current at the energies of the RHIC BES, the top RHIC energy, and at the LHC energy of 2.76 TeV. The conclusions are summarized in Sec. 5.

## 2 The magnetic field and the response of the QGP medium

One of the main issues of CME is the time evolution of the magnetic field in relativistic heavy-ion collisions. This issue has been investigated in many studies [2–5, 8, 9, 27–29], which found that enormous magnetic fields ( $B \sim 10^{15}$  T) can be generated at the very beginning of the collisions. However, according to these studies, the intensity of the magnetic field rapidly decreases with time. The higher the collision energy, the faster is the magnetic field decrease. Such a short magnetic field duration implies that the manifestation of CME in relativistic heavy-ion collisions is problematic. Recently, a limit of the magnetic field effect at late times was reported in [30–32] by studying the chiral vortex effect in relativistic heavy-ion collisions. Nevertheless, it was suggested in [8, 16] that the calculation of the magnetic field in vacuum is appropriate only for the early stage of collisions, and that the magnetic field response of the QGP medium should be considered after the formation of QGP.

Tuchin studied [33] the magnetic field properties in the QGP medium and suggested that due to the large electric conductivity, the magnetic field is partially 'frozen' during the entire plasma lifetime. The magnetic conductivity of the QGP medium was also quantitatively studied in [34–38]. We also made a study of the space-time evolution of the magnetic field in QGP in [8, 16]. The magnetic field at the center of QGP has only the y

component, and the magnitude of the magnetic field is given as

$$B_y(t \geq t_0, \mathbf{0}) = \frac{t_0}{t} e^{-\frac{c_s^2}{2a_x^2}(t^2 - t_0^2)} B_y^0(\mathbf{0}), \quad (1)$$

where  $t_0$  is the formation time of partons,  $B_y^0(\mathbf{0})$  is the magnetic field at  $t = t_0$  and at the central point ( $\vec{r} = 0$ ),  $c_s$  is the speed of sound, and  $a_x$  is the root-mean-square of the transverse entropy distribution. Here, we use  $c_s^2 \sim 1/3$  and  $a_x \sim 3$ . The formation time  $t_0$  is given as [8, 16]

$$t_0 \simeq 1/Q_s, \quad (2)$$

where  $Q_s$  is the saturation momentum, which is

$$Q_s^2 \sim A^{1/3} x^{-\varpi}, \quad x = Q_s / \sqrt{s}, \quad (3)$$

where  $A$  is the atomic number of the colliding nucleus, and  $\varpi$  is a parameter between 0.25 and 0.3 ( $\varpi = 0.3$  in this paper). The saturation momentum for different nuclei and center-of-mass energies is

$$Q_s^2(\sqrt{s}, b, A) = \left(\frac{A}{197}\right)^{\frac{2}{3(2+\varpi)}} \left(\frac{\sqrt{s}}{130}\right)^{\frac{2\varpi}{2+\varpi}} \times Q_s^2(\sqrt{s} = 130 \text{ GeV}, b, A = 197), \quad (4)$$

where  $Q_s^2(\sqrt{s} = 130 \text{ GeV}, b, A = 197)$  was given in Ref. [39]. The results for  $t_0$  and  $B_y^0(\mathbf{0})$  for two centralities and the RHIC BES and LHC collision energies are given in Table 1.

The time evolution of the magnetic field is plotted in Fig. 1 for two centralities at the RHIC BES energies, the top RHIC energy, and the LHC energy of 2.76 TeV. The magnetic fields in vacuum at different energies are also plotted for comparison. Recently, the RHIC STAR collaboration [26] presented the results of the dependence of charge correlations in the Au-Au collisions at midrapidity for center-of-mass energies of 7.7, 11.5, 19.6, 27, 39, and 62.4 GeV. It was observed [26] that the signal gradually reduces as the beam energy is decreased, and tends to vanish below 7.7 GeV after background subtraction. This suggested that hadronic interactions dominate over partonic interactions at lower collision energies. Therefore,

Table 1. Results for  $t_0$  and  $B_y^0(\mathbf{0})$  for two centralities and the RHIC BES and LHC collision energies.

$\sqrt{s}/\text{GeV}$	centrality: 10%–30%		centrality: 30%–60%	
	$t_0/\text{fm}$	$eB_y^0/\text{MeV}^2$	$t_0/\text{fm}$	$eB_y^0/\text{MeV}^2$
11.5	0.209	4275.0	0.260	6214.4
19.6	0.195	6407.1	0.242	8045.0
27	0.187	7616.7	0.232	8687.4
39	0.178	8569.5	0.221	8753.0
62.4	0.168	8481.6	0.208	7653.7
200	0.144	3980.8	0.179	2766.2
2760	0.102	579.3	0.126	156.1

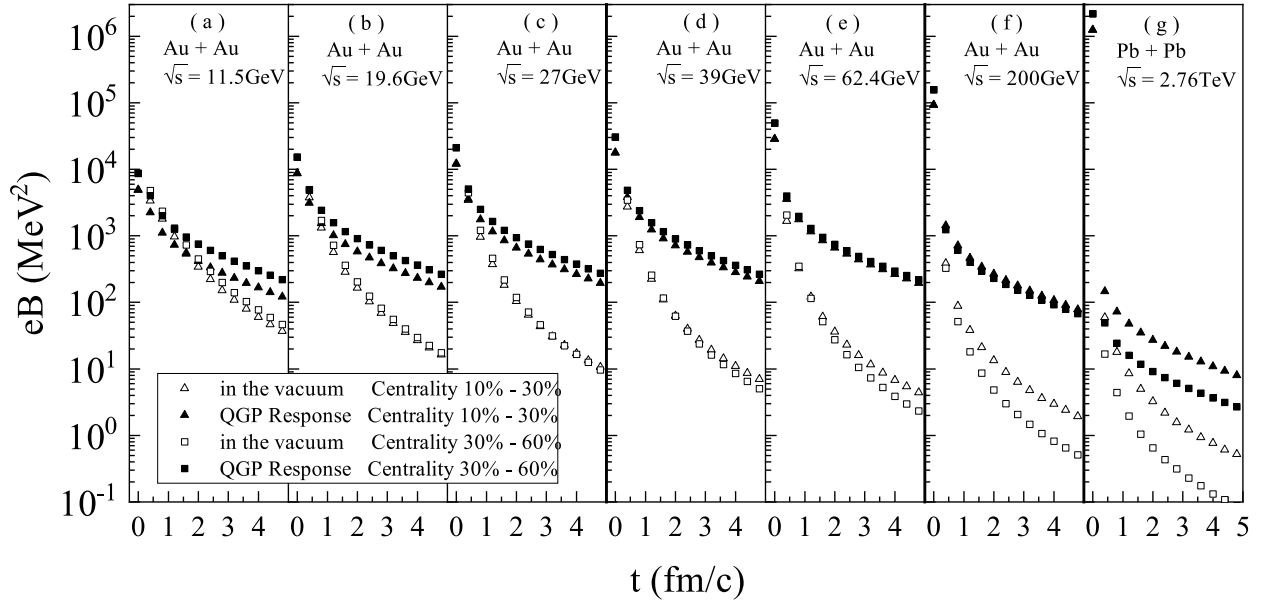


Fig. 1. Time evolution of the magnetic field for two centralities in the Au - Au collisions, for  $\sqrt{s} = 11.5, 19.6, 27, 39, 62.4, 200$  GeV, and in the Pb-Pb collisions at  $\sqrt{s} = 2760$  GeV. The solid squares and solid triangles correspond to the results in the QGP medium and for centralities of 10%~30% and 30%~60%, respectively. The hollow squares and hollow triangles are the results in vacuum with centralities of 10%~30% and 30%~60%, respectively.

the chiral magnetic effect was analyzed starting from  $\sqrt{s} = 11.5$  GeV in that article.

It is found that the magnetic fields with QGP response last longer in the 27 - 62.4 GeV energy region. Compared with the magnetic field in vacuum, the lifetime of the magnetic field is longer when the QGP medium response is considered. The strength of the magnetic field decreases rapidly with time, and the higher the collision energy, the faster is the magnetic field decrease. Compared with the RHIC energies, the initial magnetic field (at  $t = 0$ ) at the LHC energy is much bigger, but the magnetic field decreases much faster both in vacuum and with the QGP response. For the non-central collisions, the magnetic field is mainly due to the contribution of the spectator nucleus. When the two colliding nuclei are closer, the magnetic field generated is bigger, and for larger separations of the two nuclei, the magnetic field becomes smaller. For example, for the LHC energy, the spectator nucleus moves away almost at the speed of light, so that at higher collision energies, the magnetic field decreases faster.

Figure 2 shows a comparison of the time evolution of the magnetic field, normalized to its peak value, obtained in the studies by ECHO-QGP [40], Müller and Schäfer [32] (M-S) model, Deng and Huang [5] (D-H) magnetic field calculation, and in our model. The magnetic field evolution in our model decreases more rapidly than in the other models, and might induce a weaker CME signal. The results presented in the next sections are based on our model.

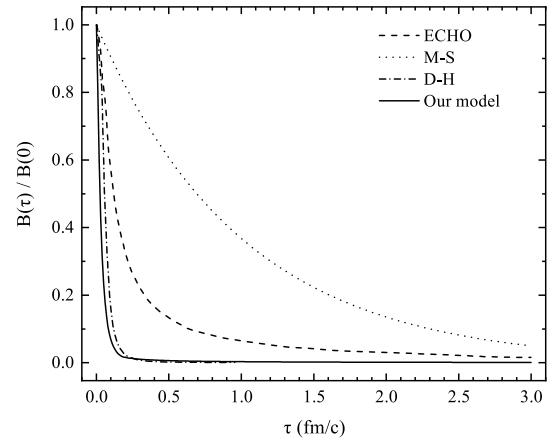


Fig. 2. Comparison of the time evolution of the magnetic field, normalized to its peak value, given in the studies: ECHO-QGP [40] (dashed line curve), M-S [32] (dotted line curve), D-H [5] (dash-dotted line curve), and in our model (real line curve).

### 3 Charge separation at the RHIC and LHC energies

In this section, we first introduce the KMW model [9], and then give a detailed analysis of CME in relativistic heavy-ion collisions at the RHIC and LHC energies.

The potential transition with non-zero winding number  $Q_w$  passes through a barrier associated with QCD which exceeds the strong coupling constant  $\alpha_s$ . The transition can be implemented by an instanton [41, 42] or

sphaleron [43, 44]. At low temperature, the transition is mainly achieved by the quantum tunneling effect, which is exponentially depressed by a transition called instanton. The transition at high temperatures is not forbidden and can be achieved by a transition called sphaleron. This may occur in the background of extremely high temperature quark gluon plasma (QGP). Thus, it provides a choice for generating chirality. On the other hand, the discovery of CME in relativistic heavy-ion collisions also implies generation of QGP.

The transition rate in QCD was given by the KMW model in Ref. [9] as follows:

$$\frac{dN_t^\pm}{d^3xdt} \equiv \Gamma^\pm \sim 192.8\alpha_s^5 T^4, \quad (5)$$

where the superscript  $\pm$  defines the transition of  $Q_w = \pm 1$ . The total transition rate is the sum of the rates of the ascending and descending transitions

$$\frac{dN_t}{d^3xdt} = \sum_{\pm} \frac{dN_t^\pm}{d^3xdt}. \quad (6)$$

In the case of a suitable magnetic field with a large temperature  $T$  and non-zero winding number  $Q_w$ , the charge separation given in Ref. [9] is

$$Q \approx 2Q_w \sum_f |q_f| \gamma(2|q_f\Phi|), \quad (7)$$

where

$$\gamma(x) = \begin{cases} x, & \text{for } x \leq 1, \\ 1, & \text{for } x \geq 1, \end{cases} \quad (8)$$

and  $\Phi = eB\rho^2$  is the magnitude of the magnetic flux.

We define by  $N_a^\pm$  and  $N_b^\pm$  the total positive/negative charge in units of  $e$  above (a) and below (b) the reaction plane, respectively.  $\Delta_\pm = N_a^\pm - N_b^\pm$  is the difference in charge between each side of the reaction plane. A charge difference will be generated locally when there is a transition from one vacuum to another. If the quarks experience many interactions in QGP, the observed final charge separation is suppressed. A suppression function

$$\xi_\pm(x_\perp) = \exp(-|y_\pm(x) - y|/\lambda) \quad (9)$$

is introduced to describe nuclear screening, where  $y_\pm(x)$  is the upper and lower  $y$  coordinate of the overlap region, and  $\lambda$  is the screening length. The expectation value of the change of  $\Delta_+$  and  $\Delta_-$  due to a transition is either positive or negative with equal probability, and is given by

$$\pm \sum_f |q_f| \gamma(2|q_f\Phi|) \xi_\pm(x_\perp), \quad (10)$$

where only the most probable transitions ( $Q_w = \pm 1$ ) are considered.

One can calculate the variation of  $\Delta_\pm$  by assuming that all transitions occur independently from each other. By using Eq. (5) and  $\rho \sim \left(\frac{\Gamma^\pm}{\alpha_s}\right)^{-\frac{1}{4}} \sim 1/(\alpha_s T)$ , we calculate

$\langle \Delta_\pm^2 \rangle$  and  $\langle \Delta_+ \Delta_- \rangle$  for small magnetic fields ( $2|q_f eB| \leq 1/\rho^2$ ). Since the magnetic field is a function of the rapidity  $\eta$ , one can compute  $\langle \Delta_\pm^2 \rangle$  and  $\langle \Delta_+ \Delta_- \rangle$  as

$$\langle \Delta_\pm^2 \rangle = 2\kappa\alpha_s \left[ \sum_f q_f^2 \right]^2 \int_{V_\perp} d^2x_\perp [\xi_-(x_\perp)^2 + \xi_+(x_\perp)^2] \times \int_{\tau_i}^{\tau_f} d\eta d\tau \tau [eB(\tau, \eta, x_\perp)]^2, \quad (11)$$

$$\langle \Delta_+ \Delta_- \rangle = -4\kappa\alpha_s \left[ \sum_f q_f^2 \right]^2 \int_{V_\perp} d^2x_\perp \xi_+(x_\perp) \xi_-(x_\perp) \times \int_{\tau_i}^{\tau_f} d\eta d\tau \tau [eB(\tau, \eta, x_\perp)]^2, \quad (12)$$

where the space-time rapidity is  $\eta = \frac{1}{2} \log[(t+z)/t-z]$ , and the proper time  $\tau = (t^2 - z^2)^{1/2}$ . The magnetic field should not alter the transition rate dramatically. There is also a constant  $\kappa$ , of the order of magnitude of one but with large uncertainties [9].  $\langle \Delta_\pm^2 \rangle$  and  $\langle \Delta_+ \Delta_- \rangle$  are connected to the correlators  $a_{++}$  ( $a_{+-}$ ) by:

$$a_{++} = a = \frac{1}{N_+^2} \frac{\pi^2}{16} \langle \Delta_\pm^2 \rangle, \quad (13)$$

$$a_{+-} = a_{-+} = \frac{1}{N_+ N_-} \frac{\pi^2}{16} \langle \Delta_+ \Delta_- \rangle, \quad (14)$$

where  $N_\pm$  is the total number of positively or negatively charged particles in the corresponding  $\eta$  interval.

Early studies of charge separation fluctuations perpendicular to the reaction plane in high energy physics experiments used the three-point correlator  $\gamma \equiv \langle \langle \cos(\phi_\alpha + \phi_\beta - 2\Psi_{RP}) \rangle \rangle$ , where the double averaging is done over all particles in an event and over all events [21, 22, 25]. Unfortunately, the  $\gamma$  correlator includes some background contributions not related to CME [45–47]. The background contribution is mainly from the elliptic flow ( $v_2$ ) in combination with the two-particle correlations. The two-particle correlator  $\delta \equiv \langle \cos(\phi_\alpha - \phi_\beta) \rangle$  was introduced to solve this problem.

By inducing  $H$  and  $F$  as CME and CME without the background contribution, one can express  $\gamma$  and  $\delta$  in the following way [46, 47].

$$\gamma \equiv \langle \cos(\phi_1 + \phi_2 - 2\Psi_{RP}) \rangle = kv_2 F - H, \quad (15)$$

$$\delta \equiv \langle \cos(\phi_1 - \phi_2) \rangle = F + H. \quad (16)$$

The  $H$  factor related to chiral magnetic signal can be obtained as:

$$H^k = (kv_2 \delta - \gamma) / (1 + kv_2), \quad (17)$$

where the coefficient  $\kappa$  ranges from 1 to 2, due to the finite detector acceptance and theoretical uncertainties [46, 47]; we take the experimental results with  $\kappa = 1.5$  in the following. A one-to-one correspondence is made between the charge separations  $a_{++}$  ( $a_{+-}$ ) of the KWM model and

the experimental results  $H_{SS}(H_{OS})$ . Therefore, the calculated result  $a_{++} - a_{+-}$  can be compared with the experimental result  $H_{SS} - H_{OS}$ , as shown in Fig. 3.

It can be seen from Fig. 3 that the model explains better the experimental data at the energies of RHIC BES and the top RHIC energy than at the LHC energy. For the Au-Au collisions at RHIC, the CME signal given by our

calculations increases from the central to peripheral collisions, and the general trend of our results is consistent with the experiment. However, for the Pb-Pb collisions at the LHC energy of  $\sqrt{s} = 2760$  GeV, the experimental CME signal [25] is very small, and only a small signal is present at the centrality of 60%~70%. Our model predicts no CME signal in this case.

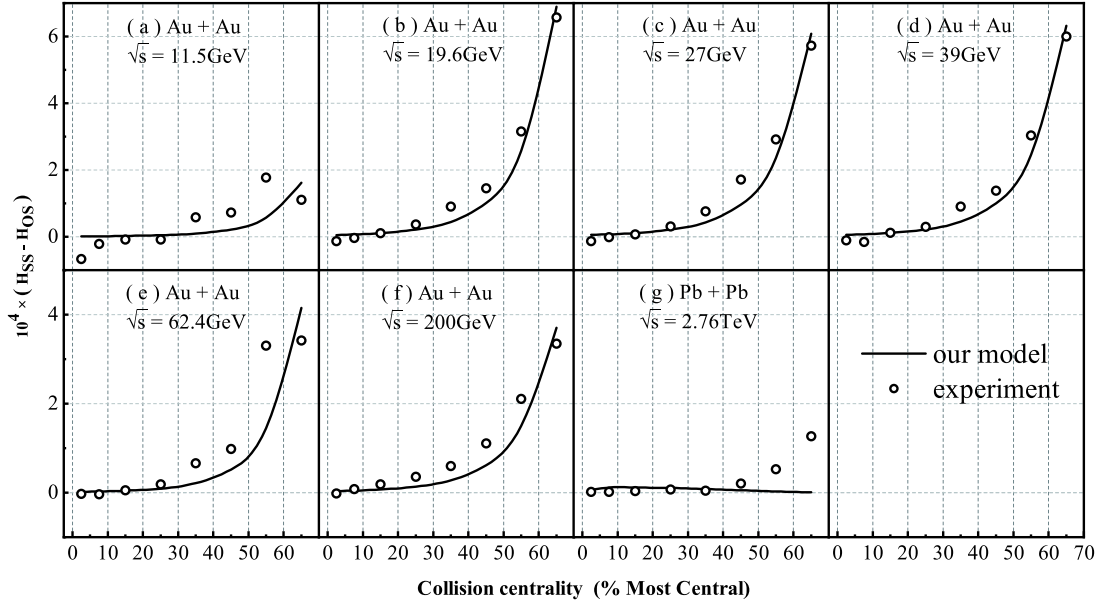


Fig. 3. Comparison between the centrality dependence of  $a_{++} - a_{+-}$  from our model and of the background subtracted experimental observable  $H_{SS} - H_{OS}$  at the RHIC and LHC energies [26].

Fig. 4 shows  $H_{SS} - H_{OS}$  as a function of beam energy for two centrality bins at the RHIC energies. The experimental results with  $\kappa = 1.5$  from Ref. [26] are used as reference for our theoretical calculations. The results in Fig. 4 show that our calculated CME signal has a very similar trend as the experimental measurements. The magnitude of our predictions is lower than the experimental data, presumably because our magnetic field decreases very quickly, as shown in Fig. 2. A quickly decreasing trend in the interval from 19.6 to 7.7 GeV is seen, which suggests that hadronic interactions dominate over partonic interactions at low beam energies. Generally speaking, our model closely follows the evolution of the magnetic field, so that our calculations include certain model limitations.

#### 4 Chiral magnetic current

Let us now turn to the induced chiral magnetic current generated by the magnetic field in the relativistic heavy-ion collisions at the RHIC and LHC energies. Assuming that the generated magnetic field has a homogen-

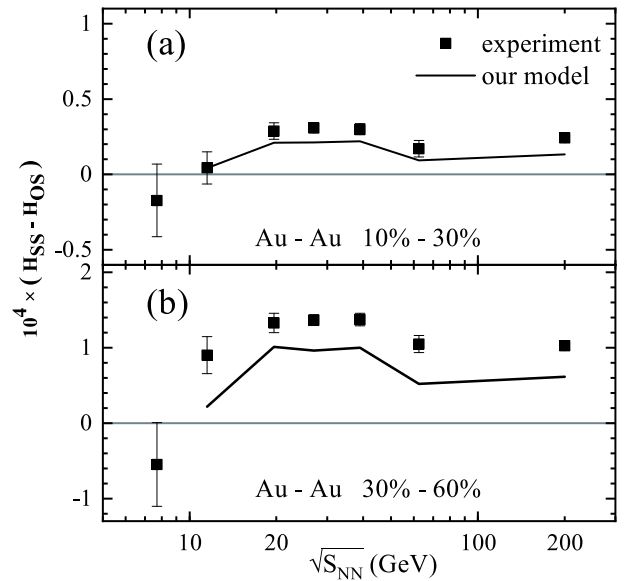


Fig. 4.  $H_{SS} - H_{OS}$  as a function of beam energy for two centrality bins at the RHIC energies. The solid curves are our calculation results. The experimental results are from Ref. [26] with  $\kappa = 1.5$ .

eous distribution, one can calculate the induced current as [16, 18]:

$$j(t) = \int_0^\infty \frac{d\nu}{\pi} \tilde{B}(\nu) [\sigma'_\chi(\nu) \cos(\nu t) + \sigma''_\chi(\nu) \sin(\nu t)], \quad (18)$$

where  $\nu$  is the frequency, and the Fourier transform of the magnetic field is given by

$$\tilde{B}(\nu) = \int_{t_0}^\infty dt B(t) e^{i\nu t}. \quad (19)$$

The real  $\sigma'_\chi(\nu)$  and imaginary  $\sigma''_\chi(\nu)$  parts of the chiral magnetic conductivity are related by the Kramers-Kronig relation

$$\sigma'_\chi(\nu) = \frac{1}{\pi} \mathcal{S} \int_{-\infty}^\infty dq_0 \frac{\sigma''_\chi(q_0)}{q_0 - \nu}, \quad (20)$$

$$\sigma''_\chi(\nu) = -\frac{1}{\pi} \mathcal{S} \int_{-\infty}^\infty dq_0 \frac{\sigma'_\chi(q_0)}{q_0 - \nu}, \quad (21)$$

where  $\sigma_\chi(\nu) = \lim_{\vec{p} \rightarrow 0} \sigma_\chi(p_0 = \nu, \vec{p})$ . The symbol  $\mathcal{S}$  in Eqs. (20) and (21) defines the integral of a singularity in the upper and the lower complex plane. The chiral magnetic conductivity should be complex, and is given as

$$\begin{aligned} \text{Im} \sum_{t=\pm} (2q + tp_0) \log \frac{(p_0 + i\varepsilon + tq)^2 - (q+p)^2}{(p_0 + i\varepsilon + tq)^2 - (q-p)^2} &= \pi [2q - |p_0| \theta(p_0^2 - p^2)] [\theta(q_+ - q) - \theta(q_- - q)] \\ &+ \pi p_0 \theta(p^2 - p_0^2) [\theta(q - q_+) - \theta(q - q_-)], \end{aligned} \quad (27)$$

where  $q_\pm = \frac{1}{2} |p_0 \pm p|$ .

After computing the real and imaginary parts of the magnetic conductivity, we use Eq. (18) to calculate the electromagnetic current. In order to use Eqs. (18) and (19), we need the dependence of the magnetic field on time after the formation of a parton. The magnetic field evolution for  $t \geq t_0$  is given by Eq. (1).

Figure 5 shows the time dependence of the induced electromagnetic current, normalized to the zero frequency chiral magnetic conductivity ( $\sigma_0 \equiv \sigma_\chi(\omega=0) = \frac{e^2}{2\pi^2} \mu_5$ ), for collisions with the centrality of 10%~30% at the RHIC and LHC energies. It can be observed that the electromagnetic current signal manifests as a strong pulse, which reaches a maximum at  $t \sim 1$  fm. The maximum value of the electromagnetic current signal directly reflects the intensity of the induced electromagnetic current. It increases with the collision energy from  $\sqrt{s} = 19.6$  GeV to  $\sqrt{s} = 39$  GeV, remains almost unchanged from  $\sqrt{s} = 39$  GeV to  $\sqrt{s} = 62.4$  GeV, and then decreases from  $\sqrt{s} = 39$  GeV to  $\sqrt{s} = 2760$  GeV.

Figure 6 is the same as Fig. 5, but for the centrality of 30%~60%. It can be seen that the maximum value of the electromagnetic current increases from  $\sqrt{s} = 19.6$  GeV to  $\sqrt{s} = 39$  GeV, and then decreases from  $\sqrt{s} = 39$  GeV to  $\sqrt{s} =$

$$\sigma_\chi(p) = \sigma'_\chi(p) + i\sigma''_\chi(p), \quad (22)$$

where both  $\sigma'_\chi(p)$  and  $\sigma''_\chi(p)$  are real functions. They can be expressed as:

$$\sigma'_\chi(p) = \frac{1}{p^i} \text{Im} R_R^i(p), \quad (23)$$

$$\sigma''_\chi(p) = -\frac{1}{p^i} \text{Re} R_R^i(p), \quad (24)$$

where  $R_R^i(p) = \frac{1}{2} \varepsilon^{ijk} \tilde{\Pi}_R^{jk}(p)$  is the retarded correlator, which can be calculated as

$$\begin{aligned} R_R^i(p) &= \frac{ie^2}{16\pi^2} \frac{p^i}{p} \frac{p^2 - p_0^2}{p^2} \int_0^\infty dq g(q) \sum_{t=\pm} (2q + tp_0) \\ &\times \log \left[ \frac{(p_0 + i\varepsilon + tq)^2 - (q+p)^2}{(p_0 + i\varepsilon + tq)^2 - (q-p)^2} \right], \end{aligned} \quad (25)$$

where

$$g(q) = \sum_{s=\pm} s (\tilde{n}(q - \mu_s) - \tilde{n}(q + \mu_s)), \quad (26)$$

and  $\tilde{n}(x) = [1 + \exp(\beta x)]^{-1}$  is the Fermi-Dirac distribution function. One can compute the imaginary part of the logarithm in Eq. (25) with  $p = |\vec{p}| \geq 0$  and  $q \geq 0$  as

2760 GeV. Figures 5 and 6 both indicate that the intensity of the induced electromagnetic current is clearly larger with the QGP response than in vacuum, and both show that the CME signal almost vanishes at the LHC energy  $\sqrt{s} = 2760$  GeV.

The dependence of the time-integrated current signal ( $Q = \int j(t) dt$ ) on the center-of-mass energy at RHIC and LHC is shown for two centralities in Fig. 7(a, b). It is found that the time-integrated current signal reaches a maximum around  $\sqrt{s} \approx 39$  GeV, and then decreases with  $\sqrt{s}$ . The qualitative trends of Figs. 5, 6, 7 are in agreement with the CME experimental results obtained at RHIC and LHC in a wide range of beam energies [26].

## 5 Summary

Considering the magnetic field response of the QGP medium, we performed a systematical study of the charge separation and compared it with the experimental results for the background-subtracted correlator  $H$  at the RHIC and LHC energies. The results show that our calculated chiral magnetic effect signal has the same trend as the experimental results at RHIC. Quantitatively, our results appear to be lower than the experimentally measured correlator

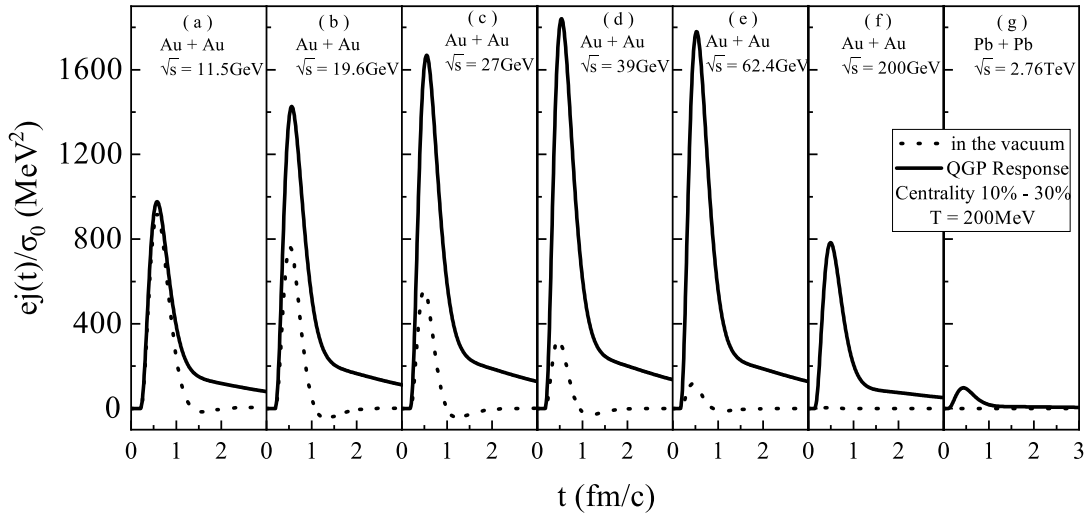


Fig. 5. Time evolution of the induced electromagnetic current, normalized to zero frequency chiral magnetic conductivity ( $\sigma_0$ ), for the RHIC and LHC collision energies. The solid curves show the results with the QGP response, and the dashed curves in vacuum. The centrality is 10%~30%.

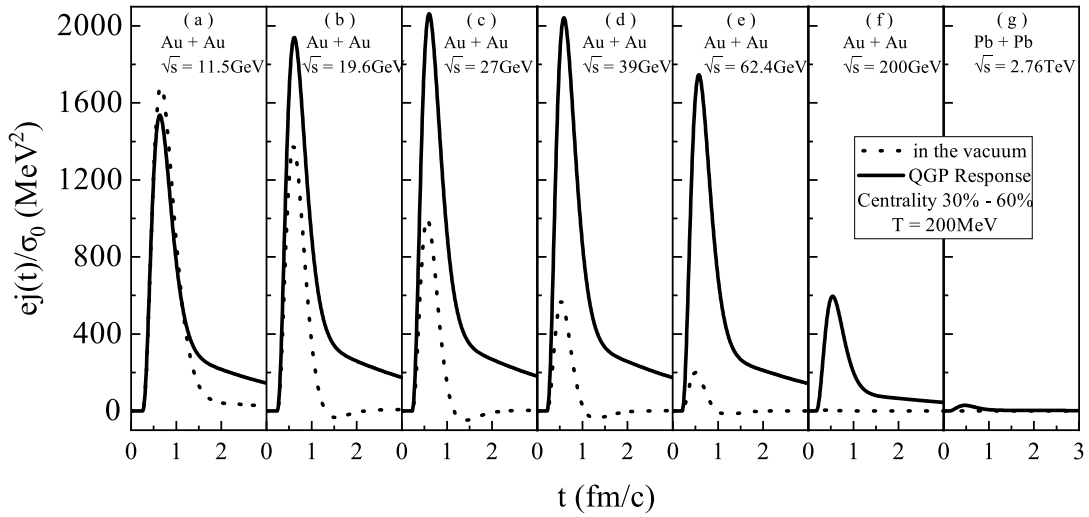


Fig. 6. As Fig.5, but for the centrality of 30%~60%.

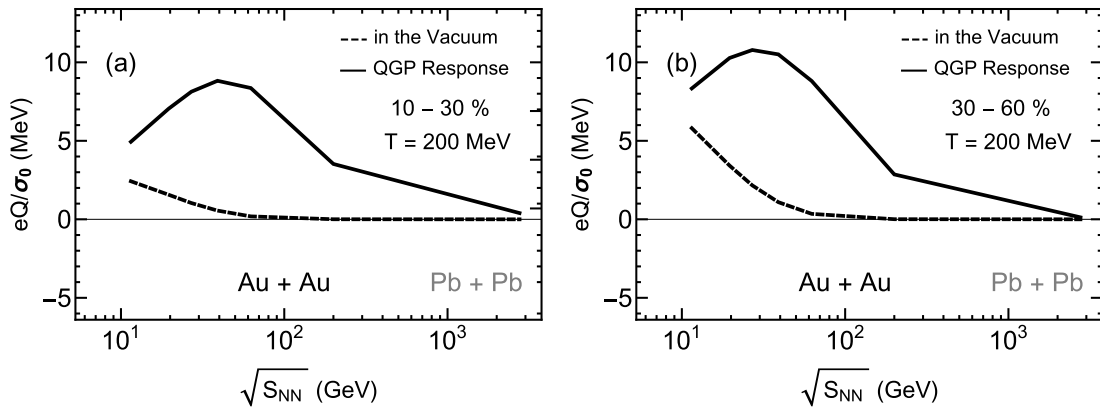


Fig. 7. Dependence of the time-integrated current signal ( $Q = \int j(t) dt$ ) on collision energy at RHIC and LHC for the centrality of 10%~30% (a), and the centrality of 30%~60% (b). The solid curves are the results with the QGP response and the dashed lines in vacuum.

ations, which may be due to the rapid decrease of the magnetic field.

The time evolution of the chiral electromagnetic current at the energies of the RHIC Beam Energy Scan and the LHC energy was systematically investigated. The dependence of the time-integrated current signal on the center-of-mass energy  $\sqrt{s}$  at RHIC and LHC and different centralities was also studied. In such a wide range of collision energies, it is important to identify the collision en-

ergy at which the electromagnetic current is largest, so as to help steer the experimental study of CME. Our phenomenological analysis showed that the time-integrated electromagnetic current has a maximum near  $\sqrt{s} \approx 39$  GeV. The qualitative trend of the induced electromagnetic current with collision energy is in agreement with the CME experimental results from RHIC and LHC [26]. We argue that the electromagnetic current at the LHC energy  $\sqrt{s} = 2760$  GeV is so small that CME cannot be produced.

## References

- 1 J. Błoczynski, X. G. Huang, X. Zhang et al, *Phys. Lett. B*, **718**: 1529 (2013)
- 2 V. V. Skokov, A. Yu. Illarionov, and V. D. Toneev, *Int. J. Mod. Phys. A*, **24**: 5925-5932 (2009)
- 3 V. Voronyuk, V. D. Toneev, W. Cassing et al, *Phys. Rev. C*, **83**: 054911 (2011)
- 4 A. Bzdak and V. Skokov, *Phys. Lett. B*, **710**: 171 (2012)
- 5 W. T. Deng and X. G. Huang, *Phys. Rev. C*, **85**: 044907 (2012)
- 6 Y. J. Mo, S. Q. Feng, and Y. F. Shi, *Phys. Rev. C*, **88**: 024901 (2013)
- 7 Y. Zhong, C. B. Yang, X. Cai et al, *Adv. High Energy Phys.*, **2014**: 193039 (2014)
- 8 S. Q. Feng, X. Ai, L. Pei et al, *Chin. Phys. C*, **42**: 054102 (2018)
- 9 D. E. Kharzeev, L. D. McLerran, and H. J. Warringa, *Nucl. Phys. A*, **803**: 227-253 (2008)
- 10 K. Fukushima, D. E. Kharzeev, and H. J. Warringa, *Phys. Rev. D*, **78**: 074033 (2008)
- 11 B. Müller and A. Schäfer, *Phys. Rev. C*, **82**: 057902 (2010)
- 12 K. F. Liu, *Phys. Rev. C*, **85**: 014909 (2012)
- 13 J. Liao, V. Koch, and A. Bzdak, *Phys. Rev. C*, **82**: 054902 (2010)
- 14 Y. Jiang, X. G. Huang, and J. Liao, *Phys. Rev. D*, **91**: 045001 (2015)
- 15 J. Liao, *Nucl. Phys. A*, **956**: 99-106 (2016)
- 16 D. She, S. Q. Feng, Y. Zhong et al, *Eur. Phys. J. A*, **54**: 48 (2018)
- 17 W. Li, S. Lin, and J. J. Mei, *Phys. Rev. D*, **98**: 114014 (2018)
- 18 D. E. Kharzeev, and H. J. Warringa, *Phys. Rev. D*, **80**: 034028 (2009)
- 19 A. Bzdak, S. Esumi, V. Koch et al, arXiv: 1906.00936[nucl-th]
- 20 D. E. Kharzeev, J. Liao, S. A. Voloshin et al, *Prog. Part. Nucl. Phys.*, **88**: 1 (2016)
- 21 B. I. Abelev et al, *Phys. Rev. Lett.*, **103**: 251601 (2009)
- 22 B. I. Abelev et al, *Phys. Rev. C*, **81**: 054908 (2010)
- 23 L. Adamczyk et al, *Phys. Rev. C*, **88**: 064911 (2013)
- 24 N. N. Ajitanand, R. A. Lacey, A. Taranenko et al, *Phys. Rev. C*, **83**: 011901 (2011)
- 25 B. Abelev et al, *Phys. Rev. Lett.*, **110**: 012301 (2013)
- 26 L. Adamczyk et al, *Phys. Rev. Lett.*, **113**: 052302 (2014)
- 27 S. Shi, Y. Jiang, E. Lilleskov et al, *Annals Phys.*, **394**: 50 (2018)
- 28 Y. Jiang, S. Shi, Y. Yin et al, *Chinese Physics C*, **42**: 011001 (2018)
- 29 A. Huang, Y. Jiang, S. Shi et al, *Phys. Lett. B*, **777**: 177 (2018)
- 30 Y. Guo, S. Shi, S. Feng et al, *Phys. Lett. B*, **798**: 134929 (2019)
- 31 X. Guo, J. Liao, and E. Wang, arXiv: 1904.04704[hep-ph]
- 32 B. Müller and A. Schäfer, *Phys. Rev. D*, **98**: 071902 (2018)
- 33 K. Tuchin, *Phys. Rev. C*, **82**: 034904 (2010)
- 34 K. Tuchin, *Adv. High Energy Phys.*, **2013**: 490495 (2013)
- 35 B. G. Zakharov, *Phys. Lett. B*, **737**: 262-266 (2014)
- 36 L. McLerran and V. Skokov, *Nucl. Phys. A*, **929**: 184-190 (2014)
- 37 K. Tuchin, *Phys. Rev. C*, **91**: 064902 (2015)
- 38 K. Tuchin, *Phys. Rev. C*, **93**: 014905 (2016)
- 39 D. Kharzeev and M. Nardi, *Phys. Lett. B*, **507**: 121-128 (2001)
- 40 G. Inghirami, L. Del Zanna, A. Beraudo et al, *Eur. Phys. J. C*, **76**: 659 (2016)
- 41 D. Diakonov, *Prog. Part. Nucl. Phys.*, **51**: 173-222 (2003)
- 42 T. Schäfer and E. V. Shuryak, *Phys. Rev. D*, **53**: 6522-6542 (1996)
- 43 P. B. Arnold and L. D. McLerran, *Phys. Rev. D*, **37**: 1020 (1988)
- 44 M. Fukugita and T. Yanagida, *Phys. Rev. D*, **42**: 1285-1286 (1990)
- 45 A. Bzdak, Koch Volker and J. Liao, *Phys. Rev. C*, **83**: 014905 (2011)
- 46 A. Bzdak, Koch Volker and J. Liao, *Lect. Notes Phys.*, **871**: 503-536 (2013)
- 47 J. Liao, *Pramana*, **84**: 901 (2015)